In-depth characterization of choline lysinate ([Cho][Lys]) in ethylene glycol for optimized CO capture conditions

Journal of Molecular Liquids 437 (2025) 128359

Contents lists available at ScienceDirect

Journal of Molecular Liquids

journal homepage: www.elsevier.com/locate/molliq

In-depth characterization of choline lysinate ([Cho][Lys]) in ethylene glycol for optimized CO_2 capture conditions

Silvia Mazzotta [a,b,d,*], Giuseppe Ferraro [c,*], Anna Vittoria De Napoli [a,c], Stefania Lettieri [c], Francesca Cardano [e], Francesca Verga [a,b], Candido F. Pirri [a,c], Sergio Bocchini [a,c]

[a] Center for Sustainable Future Technologies Istituto Italiano di Tecnologia. Via Livorno 60, Torino 10144, Italy
[b] Dipartimento di Ingegneria dell'Ambiente, del Territorio e delle Infrastrutture (DIATI) Politecnico di Torino. Corso Duca degli Abruzzi 24, Torino 10129, Italy
[c] Dipartimento di Scienza Applicata e Tecnologia (DISAT), Politecnico di Torino. Corso Duca degli Abruzzi 24, Torino 10129, Italy
[d] Scuola Universitaria Superiore (IUSS) Pavia. Palazzo del Broletto-Piazza della Vittoria 15, Pavia 27100, Italy
[e] Dipartimento di Chimica, Università di Torino. Via Pietro Giuria 7, Torino 10125, Italy

ARTICLE INFO

Keywords:
CO_2 capture
Ionic liquids
Amino acids

ABSTRACT

Choline Lysinate, an amino acid ionic liquid, demonstrates significant potential as an environmentally friendly solvent for post-combustion CO_2 capture. This study explores the physicochemical properties and CO_2 absorption performance of Choline Lysinate in ethylene glycol solutions at concentrations of 25 %, 33 %, and 50 % by weight. Key findings indicate that while the 50 % solution offers the highest CO_2 capacity, its tendency to form precipitates post-absorption renders it impractical for industrial use. The 33 % solution achieved optimal performance with a CO_2 absorption capacity of 4.45 % by weight, maintaining structural stability and thermal resistance under aging conditions. ATR-IR and TGA analyses confirmed carbamate formation during CO_2 capture and demonstrated the thermal stability of the solutions. The 25 % solution exhibited viscosity 1.3 times lower than the 33 % solution and 2.5 times lower than the 50 % solution at 30 °C, resulting in significantly reduced energy demands for solvent circulation and regeneration. Despite slightly lower CO_2 absorption (3.83 % by weight), the 25 % solution demonstrated superior energy efficiency, making it the ideal ionic liquid concentration for scalable industrial applications. These findings underscore the potential of Choline Lysinate -based solutions for sustainable CO_2 capture, offering a balance of efficiency and process stability.

1. Introduction

Carbon capture and storage (CCS) is recognized as a cornerstone of global climate mitigation strategies, addressing the urgent need to reduce greenhouse gas (GHG) emissions. The Intergovernmental Panel on Climate Change (IPCC) has consistently underscored its importance, emphasizing CCS's critical role in achieving net-zero emissions goals. With over 76 % of global emissions originating from major industrialized nations such as the United States, China, the European Union, and Japan, implementing innovative carbon capture technologies has become an international priority [1–3]' [4].

Among the various CCS methods, post-combustion CO_2 capture (PCC) stands out for its adaptability to existing industrial setups. PCC technologies primarily rely on chemical absorption processes, traditionally employing aqueous amine solutions like monoethanolamine (MEA), methyldiethanolamine (MDEA), and triethylamine (TEA). Despite their widespread use, these solvents exhibit significant limitations, including high energy demands, corrosive behavior, and susceptibility to oxidative degradation. [5–12] For instance, MEA requires approximately 3.58 GJ per ton of CO_2 for solvent regeneration, presenting a formidable energy barrier to large-scale adoption [13].

In recent years, ionic liquids (ILs) have emerged as promising alternatives to conventional amine-based solvents. As organic molten salts with melting points typically below 100 °C, ILs possess unique properties such as negligible vapor pressure, high thermal stability, and structural tunability. The stability of the IL is dictated by the nature of the cation, whereas its functional properties are primarily modulated by the selection of the anion.

In this study, we selected choline as the cation for our ILs to develop a truly sustainable CO_2 capture system. Choline, a naturally occurring quaternary ammonium compound, plays a crucial role in cellular membranes and regulates essential physiological processes. Compared

* Corresponding authors.
E-mail addresses: silvia.mazzotta@iusspavia.it (S. Mazzotta), giuseppe.ferraro@polito.it (G. Ferraro).

https://doi.org/10.1016/j.molliq.2025.128359
Received 15 January 2025; Received in revised form 10 August 2025; Accepted 18 August 2025
Available online 19 August 2025

to conventional imidazolium- and pyridinium-based ILs, choline-based ILs exhibit significantly lower toxicity due to their biological origin [14] Furthermore, choline-derived ILs can be synthesized from commercially available, renewable precursors without the use of hazardous solvents, making them an environmentally preferable alternative [15].

Our approach considers the entire supply chain, from synthesis to end-of-life regeneration, ensuring environmental compatibility, economic viability, and industrial applicability. The synthesis of our choline-based ILs relies on a metathesis reaction carried out under mild conditions, eliminating the need for energy-intensive processes (see experimental section). This choice reflects our commitment to sustainability, ensuring that our ILs are not only highly efficient in CO_2 capture but also align with green chemistry principles. With their low toxicity, biodegradability, and promising CO_2 absorption capacity, our ILs offer a practical, scalable, and environmentally responsible alternative to conventional post-combustion capture solvents.

Moreover, the tunability enables the customization of ILs for specific applications, including gas separation, catalysis, and energy storage [16,17]- [18,19]. However, despite their potential, the practical use of ILs in PCC systems has been hindered by their high viscosity, which impairs gas-liquid mixing and increases energy consumption [20–22]. Amino acid ionic liquids (AAILs) offer a compelling solution to these challenges. By combining the reactivity of amino acids with the stability of ionic liquids, AAILs facilitate efficient CO_2 capture through carbamate formation, following absorption mechanisms that vary between 1:1 and 1:2 stoichiometries depending on the specific structure of the ionic liquid (see Fig. 1). Nevertheless, their high viscosity remains a bottleneck for industrial implementation. To mitigate this issue, AAILs are often mixed with secondary solvents to reduce viscosity and enhance mass transfer efficiency [23,24].

While DMSO is a solvent known for its low toxicity, when subjected to heating, it tends to decompose, releasing compounds such as sulfuric acid and other acidic species. Over time, these byproducts can compromise its functionality due to autocatalytic reactions, accelerating the degradation process which also involves chemical decomposition, which can lead to the release of sulfuric acid and other acidic compounds [25]. A non-toxic compound such as Ethylene Glycol (EG) that at the same time is compatible with ILs and CO_2 may be the answer for a more sustainable process [26]. Although several studies have investigated ionic liquids blended with solvents for CO_2 capture, this study presents the first comprehensive investigation of [Cho][Lys] in EG. The choice of EG offers a non-toxic, biodegradable alternative with reduced solvent loss, enhancing both sustainability and process stability.

The stability of the IL is dictated by the nature of the cation, whereas its functional properties are primarily modulated by the selection of the anion.

Lysine is classified as an aminate with a polar and basic side chain that exhibits two primary amine functional groups. Since both aminates and amino acids possess a primary amine group (–NH_2), their reaction with CO_2 is expected to follow a similar mechanism, with a typical 2:1 stoichiometry of amine groups reacting with CO_2. Several experimental and computational studies have been conducted to better understand how CO_2 chemically interacts with AAILs featuring primary or secondary amine groups.

In the presence of CO_2, the ionic liquid solution consisting of cholinium cation ($[Chol]^+$) and lysinate anion ($[Lys]^-$) in EG is expected to undergo chemisorption, primarily driven by the reactivity of the amino-

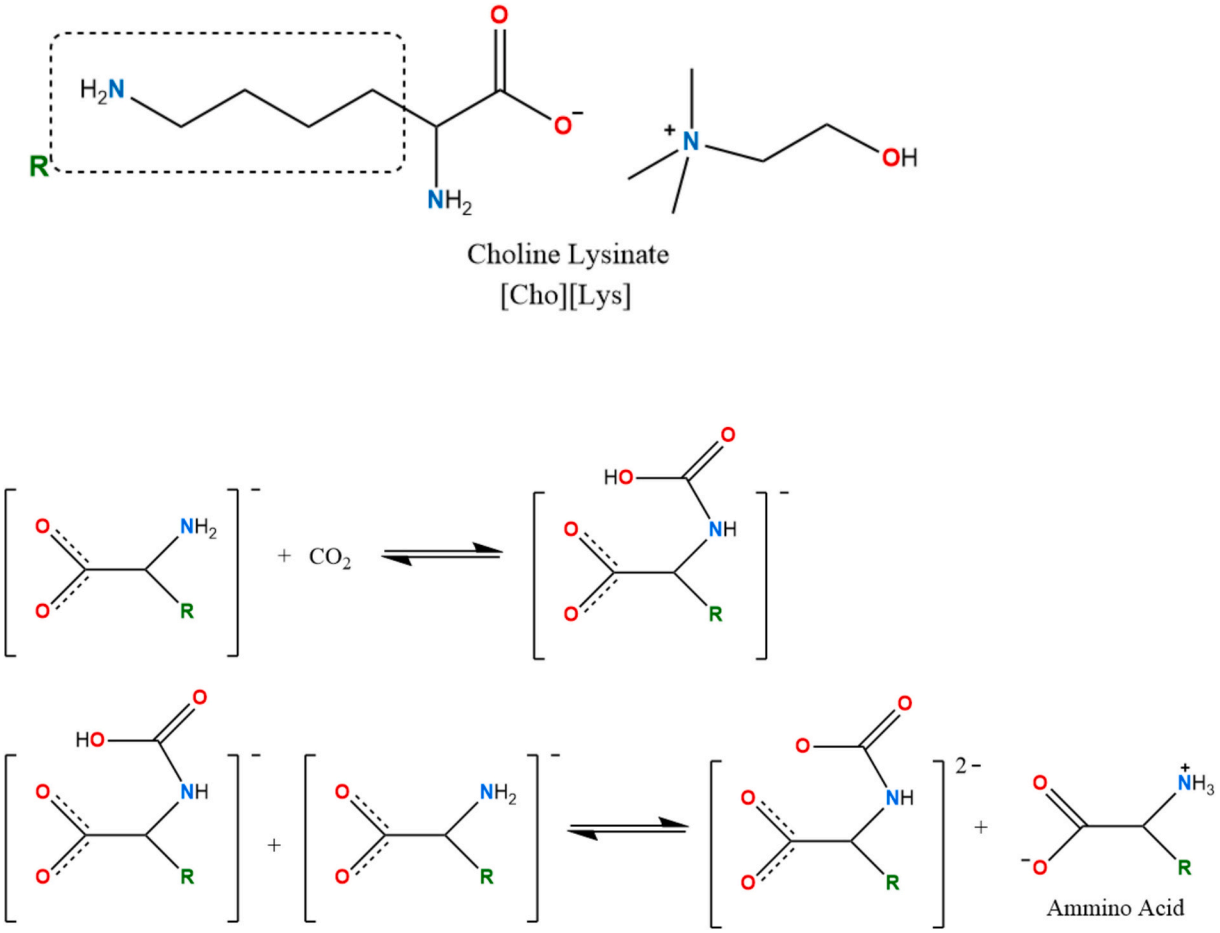

Fig. 1. - Universal reaction of CO2 with the amine group in amino-acid ILs. The cations are hidden. [27–31].

functionalized anion. The $[Lys]^-$ anion, derived from lysine, contains both primary and secondary amine groups, which serve as nucleophilic sites capable of reacting with CO_2 to form either carbamate species or carbamic acid intermediates. These reaction pathways are consistent with mechanisms proposed for other AAILs and are further illustrated in Figs. 1 and 2.

Although the $[Chol]^+$ cation does not participate directly in CO_2 capture, it plays an important structural role by contributing in the system's structural stability. It can form strong O–H···O^- hydrogen bonds with the anion, which help maintain the integrity of the ionic network. Computational studies by Madhu and Madhavan [32] demonstrated that choline tends to adopt a folded conformation, which is favorable for hydrogen bonding and promotes close contact between the cation and anion, thereby influencing the overall physicochemical properties of the IL.

The presence of EG as a polar aprotic co-solvent further enhances the system's suitability for CO_2 capture. EG acts primarily by lowering the viscosity of the pure [Cho][Lys] ionic liquid, thus facilitating greater ion mobility and improving CO_2 diffusivity throughout the solution. This results in more efficient gas–liquid contact and accelerates the absorption process. Such viscosity-lowering and performance-enhancing effects of co-solvents have also been observed in choline-based IL systems with DMSO, as reported by Shaikh et al. [33], without altering the underlying chemisorption mechanism. We expect EG to have an analogous role, promoting favorable absorption kinetics while maintaining the chemical specificity of the lysinate–CO_2 interaction.

However, the exact reaction mechanism between CO_2 and AAILs remains a topic of debate. Some studies suggest that the stoichiometric ratio could be 1:2, 1:1, or a combination of both, in accordance with the so-called 'two-reaction model.' Moreover, a specific stoichiometric ratio may only be achieved under defined external conditions (e.g., pressure, temperature). This variability can be attributed to differences in the properties of pure amino acid solutions compared to amino acids present in ILs as aminates.

Ethylene glycol, a non-toxic, biodegradable solvent, offers several advantages over conventional alternatives like water or dimethyl sulfoxide (DMSO), including lower volatility and improved compatibility with ILs [34–36]. In contrast, the use of DMSO as a co-solvent led to poor phase stability and precipitation phenomena in [Cho][Lys]-based mixtures, as shown in previous experimental work [37]. These findings highlight the superior compatibility of EG with the [Cho][Lys] system for reversible CO_2 absorption processes. By evaluating [Cho][Lys] solutions at concentrations of 25 %, 33 %, and 50 % by weight in EG, we aim to identify the optimal balance between CO_2 absorption capacity, viscosity, and thermal stability. The study provides a comprehensive analysis of the physicochemical properties of [Cho][Lys]-EG solutions, leveraging techniques such as attenuated total reflectance infrared spectroscopy (ATR-IR), thermogravimetric analysis (TGA), and CO_2 absorption tests.

Our findings contribute to advancing sustainable CO_2 capture technologies, highlighting the potential of bio-derived ionic liquids to address the dual challenges of climate change and energy efficiency. By focusing on the scalability and practicality of these solutions, we lay the groundwork for future research into amino acid-based IL systems.

2. Experimental

2.1. Materials

The amino acids L-lysine (≥97 %) and Choline Chloride (−99 %) were purchased from Sigma-Aldrich and Biosynth Carlosynth respectively. Potassium Hydroxide (KOH) (pellets) was supplied by Ensure.

The solvents Methanol (≥99.8 % (GC), ACS reagent) Ethanol (≥99.9 %), Acetonitrile (≥99.9 %), Ethylene Glycol (EG) (≥99 %), and Propylene Glycol (PG) (≥99 %) were all purchased from Sigma-Aldrich. All solvents and reagents were used as received without further purification.

Synthesis.

The choline lisinate [Cho][Lys] was synthesized via ionic metathesis, following a previously reported method [24]. Initially, 29.4 g (0.2 mol) of L-lysine were dissolved in 50 mL of methanol with 13.44 g (0.24 mol) of KOH under stirring until complete solubilization. After the addition of 27.9 g (0.2 mol) of choline chloride, a white precipitate of potassium chloride is formed. The liquid mixture was then separated from the solid particles through centrifugation (4200 rpm for 5 min). The solvent was evaporated using a rotary evaporator and then in a vacuum oven at 80 °C until constant weight recovering the raw [Cho][Lys]. The [Cho][Lys] was purified from residual inorganic salts and eventually unreacted Lysine by using an ethanol/acetonitrile 9:1 *v*/v solution and separated from the solid particles formed through centrifugation (4200 rpm for 5 min). The solution was then dried again using a rotary evaporator and then in a vacuum oven at 80 °C until constant weight. Finally, [Cho][Lys] was dried in a vacuum oven at 100 °C overnight, ensuring complete removal of free water. To prepare 25 %, 33 %, and 50 % *w*/w solutions, the ionic liquids were mixed with solvents (ethylene glycol or propylene glycol) under magnetic stirring. Prior to use, ethylene glycol (EG) was also dehydrated to eliminate residual moisture.

3. Methods

Density was determined using the pycnometer method (Eq. [1]), where *m* represents the mass of the liquid filling the pycnometer.

$$\rho = \frac{m}{V} \tag{1}$$

The volume (V) was evaluated using distilled water as the reference liquid at various temperatures. By employing the density values of water at different temperatures reported in the literature [38] the volume of the pycnometer can be derived using Eq. [2], where ρ_{ref} is the density of the reference liquid and m_{ref} is the mass of the reference liquid.

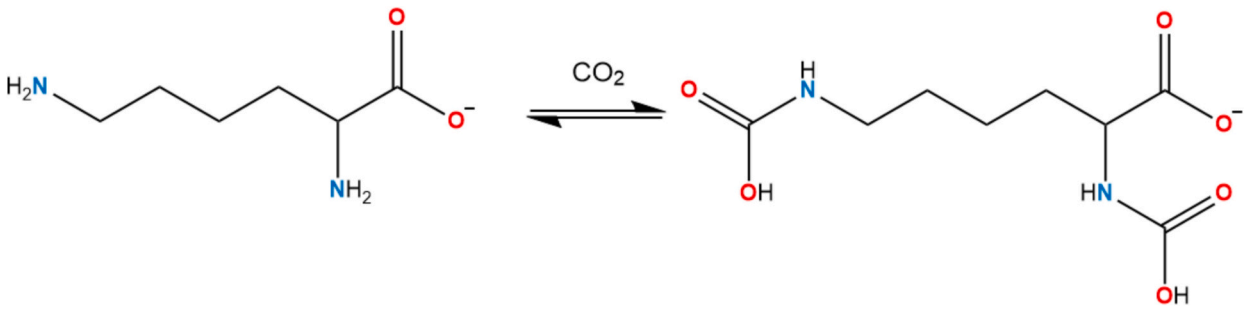

Fig. 2. - Proposed mechanism by Saravanamurugan et al. showing the reaction between CO_2 and an AAIL with two amino groups in the anion, occurring at a 2:1 M ratio [29].

$$V = \frac{m_{ref}}{\rho_{ref}} \quad (2)$$

Once the mass of the unknown liquid filling the pycnometer at different temperatures is determined, the densities of the ionic liquid solutions at various temperatures can be calculated using Eq. [1].

Viscosity. The kinematic viscosity (ν) was determined using calibrated glass capillary viscometers, specifically Cannon-Fenske viscometers. Measurements were taken at 30 °C, 40 °C, 50 °C, 60 °C, and 70 °C, following the procedure outlined in the supplementary information. The dynamic viscosity (η) of the solutions was then calculated by multiplying the kinematic viscosity (ν) by the liquid's density (ρ).

$$\eta\ (cP) = \nu(cSt)^{*}\rho\ \left(g/cm^3\right) \quad (2)$$

Specific heat capacity at constant pressure (Cp). Two primary methods exist for determining the Cp of various solutions: experimental and modeling approaches. Among the experimental methods, the differential scanning calorimeter (DSC) method is widely recognized [39,40].

The comparative method was used with the specific heat of sapphire $Cp(st)$ utilizing the differential scanning calorimeter, DSC 204 F1 Phoenix Netzsch at environment pressure. The sapphire sample for the specific heat calibration used belongs to the DSC-Set, with a diameter of 4 mm, series-no: 11323, and a thickness of 0.5 mm. Three measurements were conducted under the same conditions, with a temperature range from 0 to +90 °C, at heating rates of 10 °C min^{-1}, under an N_2 flow of 70 mL/min. All thermograms were processed using the NETZSCH Proteus® Software for Thermal Analysis. The specific heat was calculated using the following eq. [3], in accordance with the sapphire calorimetric method. Where $Wt_{st}$is the mass of the sapphire, mg, and Wt_s is the mass of the sample.

$$Cp(s) = Cp(st)^{*}\frac{D_s\ Wt_{st}}{D_{st}\ Wt_s} \quad (3)$$

$$Ds\ [J/(g{\cdot}K)\,] = mW_{sample}[mJ/sec] - mW_{empty}[mJ/sec] \quad (4)$$

$$Dst\ [J/(g{\cdot}K)\,] = mW_{saphire}[mJ/sec] - mW_{empty}[mJ/sec] \quad (5)$$

This procedure follows the guidelines of ISO 11357-4:2014, which defines the standard method for determining specific heat capacity by DSC using a sapphire reference.

ATR-IR. The ATR-IR spectra were collected using a Bruker Tensor II Fourier transform spectrophotometer equipped with a platinum ATR diamond accessory. The IR spectra were recorded at a resolution of 4 cm^{-1}, covering the spectral range from 4000 to 600 cm^{-1}. A total of 64 background scans and 32 sample scans were performed during the analysis. The spectra were subsequently processed using OPUS 8.1® software.

NMR. The NMR spectra (showed in the S.I.) were recorded on a JEOL ECZ-R 600 MHz, spectrometer at 25 °C using DMSO-d_6. Spectra were reported as chemical shifts (δ) in ppm relative to DMSO-d_6 signal as reference and processed by MNova software.

Thermal gravimetric analyses coupled with infrared spectroscopy (TGA-IR). The TGA-IR analysis were performed using a NETZSCH TG209 F1Libra thermogravimetric analyzer (TGA) coupled with a Bruker Tensor II Fourier transform spectrophotometer equipped with a DTGS detector. Approximately 25 mg of the sample were placed in an alumina open crucible and heated from 30 to 800 °C (10 °C min^{-1}) under a N_2 flow (40 mL/min). IR spectra were continuously acquired during heating in absorbance mode, with a resolution of 2 cm^{-1} in the range from 4000 to 600 cm^{-1}. The software used to process all spectra is OPUS 8.1®. Thermograms were processed using the NETZSCH Proteus® Software for Thermal Analysis.

The CO_2 absorption quantification of [Cho][Lys] and solution with EG was tested using a gravimetric method. A customized reactor with a volume of approximately 4.5 mL was used for the experiments. About 3 mL of the solution was poured into the reactor and purged with N_2 at a flow rate of 50 mL/min for 10 min to ensure an inert atmosphere. The initial weight of the solution was then recorded.

Following the N_2 purge, CO_2 was bubbled into the solution at the same flow rate of 50 mL/min until the weight of the solution ceased to increase, indicating maximum CO_2 absorption. Throughout the entire procedure, the solution was kept under continuous stirring to facilitate gas absorption.

The absorbed CO_2 was quantified by measuring the mass difference of the solution before and after CO_2 bubbling considering the headspace of the vessel (HS) in eq. 9 as the difference between total volume (V_{tot}) and the volume of solution (V_{sol}). The CO_2 absorption (CO_2 abs.) was evaluated using eq. 10, where m_{CO2} is the final weight, m_{N2} the initial mass and the weight change due to N_2 filling and CO_2 filling was evaluated by using the density of the gases (ρ) at the corresponding temperature. Two physical quantities were calculated:

1. **Absorption Capacity**: Defined as the weight ratio between the absorbed CO_2 and the liquid solution (Eq. 6).
2. **Molar Efficiency**: Defined as the molar ratio between the absorbed CO_2 and the IL present in the solution. (Eq. 7)

Details of the reactor setup and further experimental conditions can be found in the supplementary information file of our previous article [41].

$$HS = V_{tot} - V_{sol} \quad (6)$$

$$CO_2\ abs. = [m_{CO_2} - (HS^{*}\rho_{CO_2})\,] - [m_{N_2} - (HS^{*}\rho_{N_2})\,] \quad (7)$$

$$Molar\ Efficiency = \frac{CO_2\ abs/MW_{CO_2}}{m_{sol}/MW_{sol}} \quad (8)$$

4. Results and discussion

4.1. Attenuated total reflectance (ATR)

ATR measurements were performed to confirm the composition and identity of the different solutions. The spectra presented in Fig. 3 include pure [Cho][Lys], a 25 %wt [Cho][Lys] solution in EG, and pure EG. Additionally, the spectra of 33 %wt and 50 %wt [Cho][Lys] solutions are reported in ESI Fig. S1-S2.

The formation of the ionic liquid is confirmed by characteristic fingerprints of carboxylate groups, with bands appearing between 1570 and 1387 cm^{-1}. Additionally, the spectra display features indicative of neutral amine groups, which lists the principal peaks of [Cho][Lys] [42]. Specifically, abroad signal at around 3288 cm^{-1}, generated by the stretching (ν_{NH2}) of the two amine groups and the overlap of choline stretching (ν_{OH}) vibrational modes in the same spectral region along with the absence of the NH_3^+ group's stretching fingerprint, are present. The peak at 1480 cm^{-1} highlights the presence of choline since the characteristic spectral bands of choline fall within the region between 1500 and 1450 cm^{-1} [42].

In the spectrum of pure EG, all characteristic groups are observable. Notable peaks include the broad O—H stretching vibration around 3300 cm^{-1}, C—H stretching vibrations at 2933 and 2872 cm^{-1}, and the C—O stretching vibrations around 1050 cm^{-1} [43].

For the 25 %wt [Cho][Lys] solution in EG, the spectrum shows an overlap of both [Cho][Lys] and EG spectra. This is evidenced by the combined presence of the broad O—H stretching band around 3300 cm^{-1} and the distinct carboxylate and amine bands from [Cho][Lys].

The spectra of the 33 %wt and 50 %wt [Cho][Lys] solutions, as shown in ESI Figs. S1 and S2, further demonstrate the progressive increase in the intensity of the [Cho][Lys] characteristic peaks with increasing concentration, confirming the successful preparation and composition of these solutions.

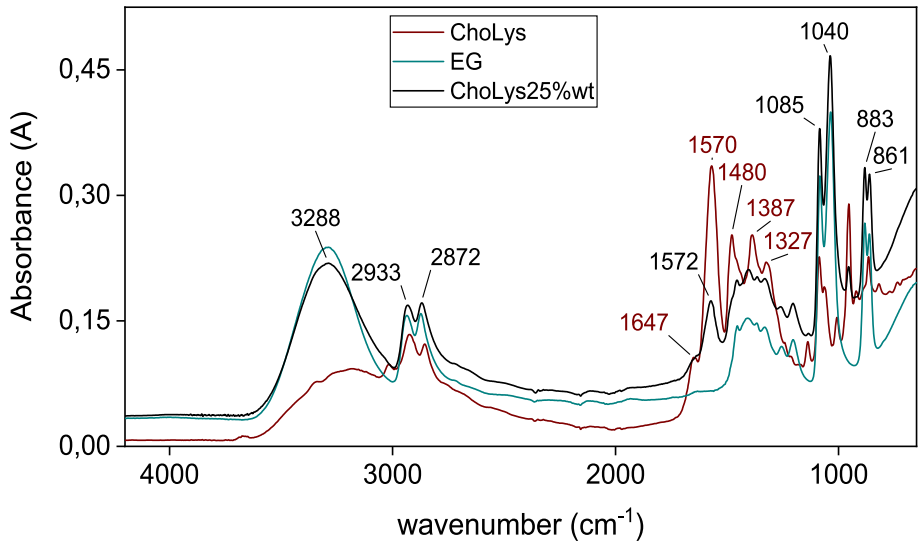

Fig. 3. - Comparison of ATR-IR spectra of [Cho][Lys] (red), EG (blue) and [Cho][Lys] solution at 25 % by weight in EG (black). (For interpretation of the references to colour in this figure legend, the reader is referred to the web version of this article.)

4.2. Thermogravimetric analyses

Pure [Cho][Lys] and its solutions at 25–33-50 %wt in ethylene glycol were characterized via TGA to assess their thermal stability and compositional characteristics. The results indicate that the ionic liquids solution exhibit an onset of thermal degradation at approximately 156 °C, with the maximum rate of degradation observed near 200 °C, see Table 1. This behavior highlights the thermal robustness of these solutions, which is crucial for industrial CO_2 capture processes.

The analysis of evolved gases during IL degradation was performed using infrared spectroscopy to gain comprehensive insights into the sample composition. Full spectra and detailed analysis are provided in Figs. S4-S8.

The TGA curve of pure [Cho][Lys] reveals four distinct weight loss steps, as shown in the first derivative of the weight loss curve with respect to temperature. The initial step occurs around 152 °C, characterized by a minor weight loss that appears as a shoulder preceding the main degradation event at 205 °C. This initial stage is attributed to the release of dimethylaminoethanol (DMAE), derived from choline decomposition, CO_2 and pentan 1–5 diamine from lysine decarboxylation. The formation of DMAE is explained by the thermal degradation of the choline cation, which undergoes fragmentation as the temperature rises. As demonstrated in previous studies on choline chloride-based systems (Latini et al.) [24] thermal stress leads to the loss of a methyl cation ($\mathbf{CH_3^+}$) from the choline cation, producing the amine-alcohol structure characteristic of DMAE. The produced methyl cation can react with nucleophylic group arrounds such as aminoacids primary amines, aminoacid anion carboxylate groups, or water, the evaporation of DMAE shift the equilibrium. This mechanism aligns with previously reported findings on choline-based ionic liquids and DESs [44], where DMAE formation is linked to the thermal instability of the choline moiety under heating conditions.

Table 1 - TGA
Analysis under N_2 flux of ionic liquids solutions in EG.

[Cho][Lys] (%wt)	T On set (°C)
25	151.6
33	161.1
50	155.4
100	135.8

The presence of DMAE is supported by spectroscopic evidence collected during the IR analysis of the evolved gases by peaks (Fig. 5S) in the C—H stretching region [45], which indicate the presence of methyl-containing molecules. Additionally, a distinctive band at 3550 cm^{-1} due to -OH stretching [45] confirming the presence of DMAE, as this feature aligns with previously reported data for dimethylethanolamine. The bands between 3500 and 4000 cm^{-1} are attributed to water evaporation and O—H stretching, while the region between 1400 and 2000 cm^{-1} includes bending modes typical of water O—H groups. Moreover the characteristic bands attributable to DMAE, matching with high fidelity the known roto-vibrational gas-phase features of DMAE. This identification is supported by the strong correspondence between our recorded spectra and the reference IR spectrum of DMAE in the gas phase [45], confirming its presence as a thermal degradation product of the choline cation, likely through a methyl group elimination pathway. The mechanism of formation from choline cation of DMAE is reported on supporting info.

The primary weight loss at 205 °C corresponds also to the decarboxylation of the lysine amino acid, leading to the release of CO_2 recognisable from the double peak around 2350 cm^{-1} for the C═O stretching in Fig. S5B [46]. A second shoulder around 265 °C follows the main degradation peak in Fig. S5C and is associated with IR bands indicative of ester formation, such as the absorption at 1708 cm^{-1} [47]. This ester is likely produced via a thermal condensation reaction between carboxylic acid from lysine and either ethylene glycol (in excess) or methyl fragments released during choline decomposition. In particular, the methyl group lost from the choline cation may participate in esterification reactions, forming volatile methyl esters under heating.

At approximately 440 °C, a further weight loss is observed, see Fig. S5D, highlighting the continued release of CO_2, dimethylaminoethanol, and trimethylamine. Additionally, the production of pentan 1,5-diamine is evident from the peak around 1626 cm^{-1}, confirming the decomposition of lysine [48].

4.3. Differential scanning calorimeter (DSC) – Heat capacity

The **heat capacity** values (Cp) are indispensable for designing and simulating absorber columns, regenerator columns, and heat exchangers in gas treatment processes. Therefore, the Cp values were determined experimentally using a DSC and employing the method of comparison with the specific heat of sapphire (see Fig. S9). As shown in Table 2, the data exhibits a trend that is directly proportional to temperature. The

Table 2
–Specific heat capacity (Cp) of [Cho][Lys]/EG solutions [j g^{-1} °C^{-1}] determined by DSC in the 20–60 °C range under nitrogen atmosphere. Measurements were performed using a sapphire standard, in accordance with ISO 11357-4:2014.

	Concentration ILs			
Temperature (°C)	25 %wt	33 %wt	50 %wt	100 %wt
20 °C	2.22	2.19	1.96	1.90
30 °C	2.26	2.24	2.00	1.93
40 °C	2.31	2.28	2.03	1.96
50 °C	2.35	2.33	2.07	2.00
60 °C	2.40	2.37	2.11	2.04

parameters of solutions at 25 %, 33 % and 50 % wt/wt of [Cho][Lys] in EG were obtained. The heat capacity decreases as the ionic liquid concentration increases. The values for the 25 % wt and 33 % wt solutions are very similar, while a more noticeable drop is observed for the 50 % wt solution.

4.4. Density and viscosity measurement

The viscosities and densities of three different IL concentration solutions in ethylene glycol were measured at multiple temperature ranging from 30 °C to 70 °C. The viscosities and densities data are showed in the Table 3.

These parameters can potentially define the ILs performance in post combustion CO_2 capture and release, as for examples a low viscosity of the IL solution promotes the mixing between gas and liquid, enhancing the overall ILs ability to capture and lately release CO_2.

The density and viscosity values of [Cho][Lys] solutions at concentrations of 25 %wt, 33 %wt, and 50 %wt were analyzed across a selected temperature range. It was observed that both density and viscosity decrease with increasing temperature. Additionally, the solution viscosity is influenced by the IL concentration. Specifically, the viscosity of the 25 %wt [Cho][Lys] solution is 1.3 and 2.5 times lower than that of the 33 %wt and 50 %wt solutions, respectively, at 30 °C. Similar trends were observed at temperatures ranging from 40 to 70 °C.

4.5. CO_2 absorption measurements

To showcase CO_2 absorption, the IL solutions were thoroughly characterized under ambient conditions using a customized instrument that regulates different gas flows into a closed reactor within a temperature-controlled chamber, with stirring provided by a magnetic stir plate.

Table 3
- Density (g cm^{-3}) e viscosity (cP) of [Cho][Lys] EG[a] solution at different temperature.

Physical Properties	Temperature	Concentration		
		25 %wt	33 %wt	50 %wt
Density [g/cm^3][b]	30 °C	1.127	1.131	1.138
	40 °C	1.122	1.125	1.134
	50 °C	1.116	1.119	1.129
	60 °C	1.113	1.112	1.122
	70 °C	1.106	1.110	1.118
Dynamic Viscosity [cp][c]	30 °C	38.844	51.520	98.065
	40 °C	24.161	33.685	62.085
	50 °C	16.433	23.063	39.745
	60 °C	11.502	15.912	25.653
	70 °C	8.547	11.293	19.270

[a] Ethylene Glycol.
[b] Measurements made using the pycnometer measurement method. Error: ±0.001.
[c] Dynamic viscosity Values were calculated with following formula: Dynamic Viscosity (cP) = Kinematic viscosity (cSt)x density (g cm^{-3}). Kinematic viscosity values were determined by Cannon-Fenske viscometers.

The amount of CO_2 absorbed by the IL-solvent systems was assessed using a gravimetric approach to measure the CO_2/N_2 molar efficiency and gas absorption percentage (Table 4). A 1.5 mL solution was placed in a 5 mL reactor. Several CO_2 absorption tests were conducted using various CO_2 percentage fluxes, specifically 25 %, 50 %, 75 %, and 100 % CO_2/N_2, with a total flow rate of 20 mL/min.

The CO_2 capacity was estimated by the difference in mass before and after exposure to the gas, considering the contribution from the headspace in the reactor. The CO_2 loading was defined as the percentage of CO_2 captured over the total mass of the IL solution. Molar efficiency was defined as the molar ratio between the captured CO_2 and the quantity of IL.

The mol (NH_2) was calculated considering impurities. The molar efficiency of IL solutions exhibits inversely proportional trends with ILs concentrations. Specifically, under 100 % CO_2 gas flux, the molar efficiency of [Cho][Lys] 25 %wt is 0.44. [Cho][Lys] 33 %wt has a molar efficiency of 0.38, and [Cho][Lys] 50 %wt shows a molar efficiency of 0.29. Although [Cho][Lys] 50 wt% shows the highest CO_2 absorption capacity among the tested formulations (Table 5), a white precipitate was observed in the solution after saturation. This indicates that the absorption process is not fully reversible in this case. While a precise identification of the solid phase was not possible due to the high viscosity of the solution and the fine dispersion of the precipitate, two hypotheses can be proposed: (i) precipitation of lysine amino acid, potentially released from the lysinate anion upon CO_2 reaction, and (ii) formation and aggregation of a neutral CO_2 adduct, such as a carbamate or carbonate species, with limited solubility in ethylene glycol. The intimate mixing and strong interactions within the viscous liquid phase prevented isolation of the solid for further analysis, but the loss of reversibility suggests that such phase separation plays a role in the retention of CO_2 in this system. Consequently, despite the 50 % by weight solution of [Cho][Lys] in EG showing a higher absorption capacity, these tests suggest that the most promising solution is [Cho][Lys] in ethylene glycol at 33 % by weight. The absorption capacity is 4.45, and no precipitates form during the absorption tests.

Table 5 summarizes experimentally measured CO_2 solubility data for ionic liquids with lysinate anions, as reported in the literature, facilitating a comparative evaluation with our study. Notably, our [Cho][Lys]-EG solutions achieve superior gravimetric CO_2 uptake, reaching values as high as 3.27 mol CO_2/kg IL at 25 % wt concentration under ambient conditions. This represents a significant advancement compared to previously studied lysinate-based systems, including aqueous formulations (e.g., 2.20 mol CO_2/kg IL for aqueous [Cho][Lys]) and other ethylene glycol-based ionic liquids (e.g., 1.0501 mol CO_2/kg IL for [N1111][Lys] at 50 % wt).

The practical advantage of using ethylene glycol as a solvent lies in its negligible volatility, biodegradability, and compatibility with ionic liquids, which substantially reduces solvent loss and simplifies the regeneration process compared to aqueous or volatile organic solvents. Consequently, our [Cho][Lys]-EG solutions not only demonstrate higher CO_2 absorption capacities but also present enhanced sustainability and operational efficiency, making them promising candidates for

Table 4
- Absorption capacity values of [Cho][Lys] 25, 33 and 50 % by weight in ethylene glycol conducted at a temperature of 25 °C with a flow of 20 mL/min of a CO_2/N_2 gas mixture at 25, 50, 75, 100 % CO2.

CO_2 absorption [a] at different CO_2/N_2 gas mixture					
[Cho][Lys] (% *w*/w)	25 %	50 %	75 %	100 %	Notes
25	2.89	3.21	3.28	3.83	No changes detected
33	3.01	3.36	3.64	4.45	No changes detected
50	4.39	4.90	5.45	5.12	White precipitate forms

a Expressed as %wt (wt of solution after CO_2 absorption test on wt of (solution before CO_2 absorption test).

Table 5
Examples of experimentally measured CO_2 solubility in ionic liquids with lysine as the anion reported in literature.[a, d]

ILs	Solvent	Pressure (bar)	CO_2 uptake (mol CO_2/mol IL)	mol CO_2/kg IL	Reference
[Cho][Lys]					
25 %wt	EG	1	0.81 [a]	3.27 [a]	Our work
33 %wt			0.77 [a]	3.09 [a]	
50 %wt			0.58 [a]	2.34 [a]	
15 %[N1111][Lys] + 15 % MDEA	Water	1	0.69–0.74 [b]		[49]
[Cho][Lys]	Water	1	2.20 [c]		[50]
[VBIm][Lys]	–	–	0.204 [d]		[30]
MDEA/[C2OHmim][Lys]	water	–	0.75 [e]		[51]
[N1111][Lys]					
20 %wt	EG	1.01	-	0.5637 [f]	[52]
50 % wt			-	1.0501 [f]	

[a] The error was estimated by propagation, accounting for the instrument's sensitivity, with the balance resolution at a maximum of 0.1 mg. Additionally, the trends in the measured values were analyzed, and the associated curves were estimated (see SI under 'Absorbance Trend Estimation' section).
[b] $P = 97$ kPa, $T = 298$ K. Uptake capacity (mol CO_2 * $mol_{amines} - 1$) IL + MDEA solutions of 30 % total amines.
[c] Aqueous solution with 50 wt% of cholinium lysinate.
[d] Abs at $T = 303.15$ K; $P = 0.978$ CO_2: 10 % (v/v); cIL: 0.4 mol·L^{-1}.
[e] MDEA (0.2 mol/L) and [C_2OHmim][Lys] (0.8 mol/L). Blended absorbents of a molar ratio of 8:2 of MDEA/[C_2OHmim][Lys].
[f] CO_2 Load of AAILs at 303 K expressed in mol CO_2/Kg IL solution.

industrial-scale, sustainable CO_2 capture applications.

4.5.1. Post-absorption ATR analysis

To better understand the IL-CO_2 interaction, ATR measurement was performed also after gravimetric absorption test.

As showed in Fig. 4, the comparison of ATR-IR spectra before and after the gravimetric absorption test reveals three distinct peaks, confirming the formation of carbamic acid and carbamate anion. The peak at 2337 cm^{-1} indicates the presence of CO_2, typically appearing as a double peak in gas physisorption solutions, though in this case, the two peaks converge into a single peak. At 1635 cm^{-1}, the vibrational stretching mode of the C═O bond in ammonium carbamate is observed. The peak at 1294 cm^{-1} is attributed to the symmetric stretching of the COO^- group in carbamate. Additional evidence of carbamic acid and carbamate formation would have been the disappearance of the peak corresponding to the N—H group stretching at 3200 cm^{-1}, unfortunately obscured by overlap with the broad band of the solvent's hydroxyl group [53,54]. In Fig. S10, and S11 the comparison of ATR-IR spectra before and after the gravimetric absorption test of [Cho][Lys] 33 %wt and [Cho][Lys]50 %wt in Ethylene Glycol are reported.

4.5.2. Post-absorption TGA

In Table S1 in the ESI, the values of onset temperature (T_on set) and the temperature corresponding to the maximum degradation rate for the IL solutions after undergoing CO_2 capture tests are presented. The tests were conducted over a temperature range from 30 °C to 800 °C, with a heating rate of 20 K/min and a constant nitrogen flow of 40 mL/min. The data reveals a clear trend in the thermal degradation characteristics of the IL solutions. As the concentration of [Cho][Lys] increases, both the onset temperature and the maximum degradation rate decrease. The 25 % solution has the highest onset temperature (192 °C) and maximum degradation rate, indicating greater thermal stability compared to the higher concentrations. In contrast, the 33 % and 50 % solutions have lower onset temperatures and similar degradation profiles, suggesting a decrease in thermal stability with increasing concentration, see Fig. S12 and Fig. S13.

This information indicates that while the IL solutions demonstrate substantial degradation, both the 25 % and 33 % concentrations maintain a relatively stable profile under thermal conditions compared to the higher concentration (see Fig. 3). Thermograms of [Cho][Lys] solutions at 25 %wt and 50 %wt in EG, obtained after the CO_2 absorption test, are available in Fig. S12 and S13.

4.6. Evaluation of CO_2 absorption stability in aged [Cho][Lys] 33 %wt solution

Having selected the 33 %wt [Cho][Lys] solution in EG as the candidate, due to its higher CO_2 absorption (Table 5) and thermal stability (Fig. 3), it underwent an aging process before its absorption capacity was remeasured, confirming the values presented in Table 6. The CO_2 absorption test was conducted on the aged [Cho][Lys] 33 %wt solution in EG. The aging process involved exposing the ionic liquid solution to constant atmospheric airflow during heating at 80 °C for one week, as illustrated in Fig. S14 of the ESI. During this process, degradation was primarily driven by two factors: oxidative stress induced by

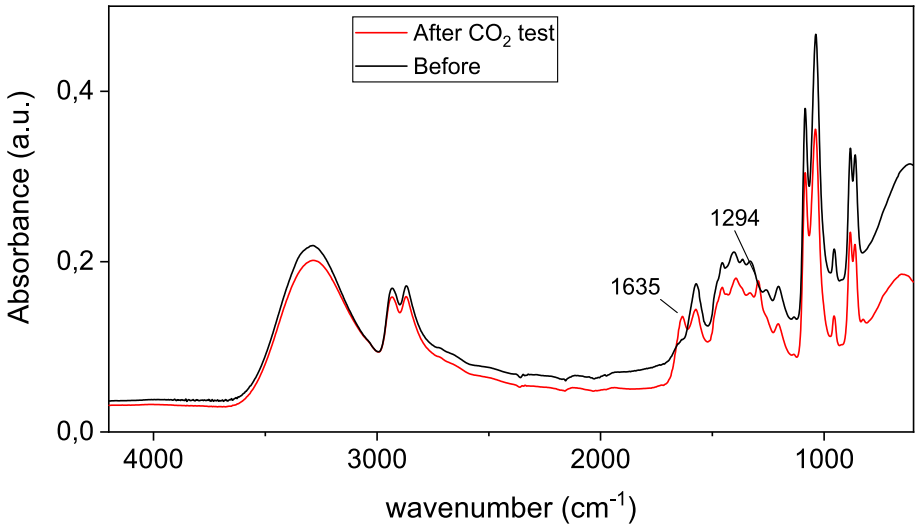

Fig. 4. Comparison of ATR-IR spectra of [Cho][Lys] 25 % wt in ethylene glycol, before and after the gravimetric absorption test, performed by exposing the ionic liquid solution to a 30 mL/min CO_2 flow.

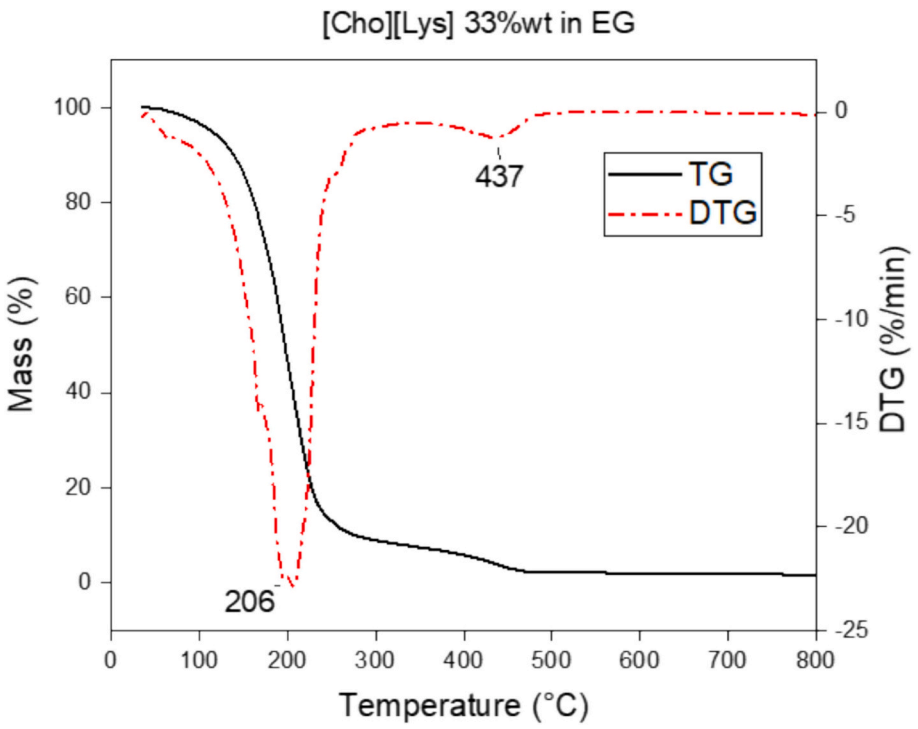

Fig. 5. - Thermogram of the [Cho][Lys] solution at 33 %wt in Ethylene Glycol obtained after the CO_2 absorption test.

Table 6 - CO_2 absorptions in solutions at 33 % by weight of ILs in solvent.

ILs solution in EG[a]	CO_2 capacity [b]		Notes
	100 % flux CO_2		
ChLys33%wt	Before aging process [c]	4.45	No changes detected
	After aging process [c]	4.84	No changes detected

[a] Ethylene Glycol.
[b] Expressed as %wt(wt (solution after CO_2 absorption test)/wt(solution before CO_2 absorption test)).
[c] The aging process involved exposing the ionic liquid solution to a constant airflow for one week.

atmospheric oxygen and thermal effects due to sustained heating.

After a week, some of the solvent had evaporated, necessitating a refill of solvent before proceeding with the CO_2 capture test. The test was conducted according to the previously reported methodology, and the results are summarized in Table 6. The results indicate that the CO_2 absorption capacity of the aged [Cho][Lys] 33 %wt solution is comparable before and after the aging process. These values suggest that the aging process maintains the ionic liquid's effectiveness in absorbing CO_2, potentially due to consistent structural integrity and favorable interactions within the solution. The retention of absorption capacity is a promising result for the long-term application of this ILs in CO_2 capture.

To evaluate the regeneration capability and stability of the [Cho][Lys]/EG system upon repeated use, a multi-cycle CO_2 absorption test was carried out. As shown in **Fig. S15** (Supporting Information), the second absorption cycle proceeds with a significantly steeper decline in CO_2 concentration compared to the first one, indicating enhanced kinetics and faster uptake.

This qualitative improvement suggests that the system undergoes a favorable structural or diffusional rearrangement after the initial CO_2 exposure. Such behavior has also been reported for amino-acid ionic liquids in DMSO-based systems, where conditioning after the first cycle led to improved gas-liquid interaction efficiency [55].

These findings reinforce the potential of [Cho][Lys] in EG not only as an effective absorbent, but also as a reusable and low-maintenance material for cyclic CO_2 capture applications.

5. Conclusion

The use of EG as a solvent represents a notable improvement over traditional volatile solvents such as DMSO. EG's lower vapor pressure minimizes solvent loss, while its compatibility with ionic liquids enhances solution stability. This improved sustainability, coupled with its superior viscosity profile, underscores EG's potential for scalable CO_2 capture applications. By reducing solvent volatility and improving thermal stability, EG offers an environmentally friendly alternative that aligns with industrial requirements for long-term CO_2 capture processes.

In this comprehensive study, we investigated the performance of [Cho][Lys] for CO_2 capture applications, with a particular focus on how dilution of the IL can enhance efficiency. Both the 25 % wt and 33 % wt solutions in EG demonstrated comparable CO_2 capture performance, highlighting their viability for practical use. However, the 50 % wt solution exhibited signs of precipitation, indicating that higher concentrations may not be suitable for scalable applications.

Our findings suggest that the 25 % wt solution offers the best combination of efficiency, stability, and energy savings. Despite the slightly lower CO_2 absorption capacity compared to the 33 % wt solution, the 25 % wt formulation demonstrated significantly lower viscosity, reducing the energy demands associated with solvent circulation and regeneration. This property makes the 25 % wt solution a more viable candidate for large-scale industrial applications, where minimizing energy costs is crucial.

Furthermore, an aging test confirmed that the 33 % wt solution retains its CO_2 absorption capacity even after prolonged exposure to oxidative and thermal conditions. This result underscores the stability and robustness of this IL formulation, strengthening its suitability for long-term use in demanding operational environments.

Considering the promising performance of both the 25 % wt and 33 % wt solutions, we recommend expanding future research to explore other AAILs combined with EG to further optimize CO_2 capture performance. Using the 25 % wt concentration as the baseline for these investigations will ensure an optimal balance of absorption capacity,

viscosity control, and energy efficiency for scalable applications. By combining environmentally friendly solvents like EG with bio-derived ionic liquids, this study contributes to advancing sustainable and effective CO_2 capture technologies for industrial applications.

CRediT authorship contribution statement

Silvia Mazzotta: Writing – review & editing, Writing – original draft, Investigation, Data curation. **Giuseppe Ferraro:** Methodology, Investigation, Data curation, Conceptualization. **Anna Vittoria De Napoli:** Investigation, Data curation. **Stefania Lettieri:** Writing – review & editing, Supervision. **Francesca Cardano:** Visualization, Investigation, Data curation. **Francesca Verga:** Supervision. **Candido F. Pirri:** Resources, Funding acquisition. **Sergio Bocchini:** Writing – review & editing, Supervision.

Declaration of competing interest

The authors declare that they have no known competing financial interests or personal relationships that could have appeared to influence the work reported in this paper.

Acknowledgements

This study was carried out within the Agritech National Research Center and received funding from the European Union Next-GenerationEU (PIANO NAZIONALE DI RIPRESA E RESILIENZA (PNRR) – MISSIONE 4 COMPONENTE 2, INVESTIMENTO 1.4 – D.D. 1032 June 17, 2022, CN00000022). Furthermore, authors wish to thank European Union for the financial support through the Next Generation EU- projects “Nord Ovest Digitale E Sostenibile-NODES” (PNRR, D.D. n.1054 June 23, 2022), NEST “Network for Energy Sustainable Transition- NEST”(PE0000021, D.D. n.341 March 15, 2022) and PNRR Mission 4 “Education and Research”—Component 2 “From research to business”—Investment 3.1 “Fund for the realization of an integrated system of research and innovation infrastructures”—Call for tender No. n. 3264 of 28/12/2021 of Italian Ministry of Research funded by the European Union—NextGenerationEU—Project code: IR0000027, Concession Decree No. 128 of 21/06/2022 adopted by the Italian Ministry of Research, CUP: B33C22000710006, Project title: iENTRANCE. Authors also acknowledge Ministero dello Sviluppo Economico (MISE) and Ministero della Transizione Ecologica (MITE) for the financial support. This manuscript reflects only the authors’ views and opinions, neither the European Union nor the European Commission can be considered responsible for them.

This paper and related research have been conducted during and with the support of the Italian national inter-university PhD course in Sustainable Development and Climate change (link: www.phd-sdc.it).

Appendix A. Supplementary data

Supplementary data to this article can be found online at https://doi.org/10.1016/j.molliq.2025.128359.

Data availability

Data will be made available on request.

References

[1] M. Honegger, Nat. Commun. 14 (2023).
[2] H. Kheshgi, H. de Coninck, J. Kessels, Mitig. Adapt. Strateg. Glob. Chang. 17 (2012) 563.
[3] S. Paltsev, J. Morris, H. Kheshgi, H. Herzog, Appl. Energy 300 (2021).
[4] C. Intergovernmental Panel on Climate, Climate Change 2022 - Mitigation of Climate Change, 2023.
[5] K.A. Mumford, Y. Wu, K.H. Smith, G.W. Stevens, Front. Chem. Sci. Eng. 9 (2015) 125.
[6] T. Wilberforce, A. Baroutaji, B. Soudan, A.H. Al-Alami, A.G. Olabi, Sci. Total Environ. 657 (2019) 56.
[7] A. Kamolov, Z. Turakulov, S. Rejabov, G. Diaz-Sainz, L. Gomez-Coma, A. Norkobilov, M. Fallanza, A. Irabien, Membranes (Basel) 13 (2023).
[8] J.E. Bara, D.E. Camper, D.L. Gin, R.D. Noble, Acc. Chem. Res. 43 (2010) 152.
[9] J. de Riva, J. Suarez-Reyes, D. Moreno, I. Díaz, V. Ferro, J. Palomar, International Journal of Greenhouse Gas Control 61 (2017) 61.
[10] S. Bocchini, C. Castro, M. Cocuzza, S. Ferrero, G. Latini, A. Martis, F. Pirri, L. Scaltrito, V. Rocca, F. Verga, D. Viberti, J. Nanomater. 2017 (2017) 1.
[11] S. Seo, L.D. Simoni, M. Ma, M.A. DeSilva, Y. Huang, M.A. Stadtherr, J.F. Brennecke, Energy Fuel 28 (2014) 5968.
[12] B. Aghel, S. Janati, S. Wongwises, M.S. Shadloo, International Journal of Greenhouse Gas Control 119 (2022).
[13] H. Huang, R. Peters, R.C. Samsun, D. Stolten, C. He, X. Zhou, Energy 301 (2024).
[14] H.J. Jiang, S. Miao, S. Imberti, B.A. Simmons, R. Atkin, G.G. Warr, Green Chem. 23 (2021) 856.
[15] S. Bhattacharyya, F.U. Shah, ACS Sustain. Chem. Eng. 4 (2016) 5441.
[16] J.E. Bara, Absorption-Based Post-Combustion Capture of Carbon Dioxide, 2016.
[17] S.F. Cannone, M. Tawil, S. Bocchini, M. Santarelli, Carbon Capture Science & Technology 13 (2024).
[18] J. Lu, J. Zhang, X. Wang, J. Zhang, Z. Tian, E. Zhu, L. Yang, X. Guan, H. Ren, J. Wu, X. Li, G. Wang, J Energy Storage 103 (2024).
[19] S. Kirchhecker, D. Esposito, Current Opinion in Green and Sustainable Chemistry 2 (2016) 28.
[20] V.S. Detlef Stolten, Efficient Carbon Capture for Coal Power Plants, 2011.
[21] J. Palomar, J. Lemus, P. Navarro, C. Moya, R. Santiago, D. Hospital-Benito, E. Hernandez, Chem. Rev. 124 (2024) 1649.
[22] B. Gurkan, B.F. Goodrich, E.M. Mindrup, L.E. Ficke, M. Massel, S. Seo, T.P. Senftle, H. Wu, M.F. Glaser, J.K. Shah, E.J. Maginn, J.F. Brennecke, W.F. Schneider, The Journal of Physical Chemistry Letters 1 (2010) 3494.
[23] M. Hosseinpour, M.J. Shojaei, M. Salimi, M. Amidpour, Fuel 353 (2023).
[24] G. Latini, M. Signorile, F. Rosso, A. Fin, M. d’Amora, S. Giordani, F. Pirri, V. Crocellà, S. Bordiga, S. Bocchini, J CO_2 Util 55 (2022).
[25] Q. Yang, M. Sheng, J.J. Henkelis, S. Tu, E. Wiensch, H. Zhang, Y. Zhang, C. Tucker, D.E. Ejeh, Org. Process. Res. Dev. 23 (2019) 2210.
[26] R.B. Leron, M.-H. Li, Thermochim. Acta 551 (2013) 14.
[27] Q. Yang, Z. Wang, Z. Bao, Z. Zhang, Y. Yang, Q. Ren, H. Xing, S. Dai, ChemSusChem 9 (2016) 806.
[28] B. Gurkan, B. Goodrich, E. Mindrup, L. Ficke, M. Massel, S. Seo, T. Senftle, H. Wu, M. Glaser, J. Shah, The Journal of Physical Chemistry Letters 1 (2010) 3494.
[29] A.S. Gouveia, L.C. Tome, I.M. Marrucho, J. Chem. Eng. Data 61 (2016) 83.
[30] X. Liu, Y. Wang, M. He, Process. Saf. Environ. Prot. 185 (2024) 1319.
[31] N. Noorani, A. Mehrdad, I. Ahadzadeh, Fluid Phase Equilib. 547 (2021) 113185.
[32] D.K. Madhu, J. Madhavan, J. Mol. Liq. 249 (2018) 637.
[33] A.R. Shaikh, A. Grillo, M.C. D’Alterio, J.J. Pajski, S.I. Amran, H. Karim, M. Chawla, G. Talarico, A. Poater, L. Cavallo, J. Mol. Liq. 424 (2025) 127084.
[34] F. Felix, L.A.J. Letti, G. Vinicius de Melo Pereira, P.G.B. Bonfim, V.T. Soccol, C. R. Soccol, Crit. Rev. Biotechnol. 39 (2019) 1031.
[35] S. Talekar, A.F. Patti, R. Singh, R. Vijayraghavan, A. Arora, Ind. Crop. Prod. 112 (2018) 790.
[36] M. D’Este, M. Alvarado-Morales, I. Angelidaki, Biotechnol. Adv. 36 (2018) 14.
[37] G. Latini, DISAT, Politecnico di Torino, Italy, 2021.
[38] S.W.A.T.E.C, Water - Density, 2003.
[39] J. McHugh, P. Fideu, A. Herrmann, W. Stark, Polym. Test. 29 (2010) 759.
[40] I. Blanco, Thermochim. Acta 685 (2020).
[41] G. Latini, M. Signorile, V. Crocellà, S. Bocchini, C.F. Pirri, S. Bordiga, Catal. Today 336 (2019) 148.
[42] A. Barth, Prog. Biophys. Mol. Biol. 74 (2000) 141.
[43] Y.-C. Guo, C. Cai, Y.-H. Zhang, AIP Adv. 8 (2018).
[44] N. Delgado-Mellado, M. Larriba, P. Navarro, V. Rigual, M. Ayuso, J. García, F. Rodríguez, J. Mol. Liq. 260 (2018) 37.
[45] S.-A.C, LLC, Wiley, 2025.
[46] N.I.O.S.A. Technology, U.S. Departement of Commerce, 2025.
[47] D.L. Pavia, G.M. Lampman, G.S. Kriz, J.A. Vyvyan, Introduction to Spectroscopy, Cengage Learning, 2008.
[48] I. John Wiley & Sons, Wiley, 2025.
[49] Z. Feng, F. Cheng-Gang, W. You-Ting, W. Yuan-Tao, L. Ai-Min, Z. Zhi-Bing, Chem. Eng. J. 160 (2010) 691.
[50] F. Ramondo, S. Di Muzio, Entropy (Basel) 24 (2022).
[51] W. Kong, Z. Chen, F. Liu, K. Yang, Y. Shen, S. Zhang, W. Li, S. Li, Sep. Purif. Technol. 326 (2023).
[52] M. Chen, M. Li, L. Zhang, X. Liu, F. Zhang, Y. Wu, ACS Sustain. Chem. Eng. 10 (2022) 12082.
[53] B.E. Gurkan, J.C. de la Fuente, E.M. Mindrup, L.E. Ficke, B.F. Goodrich, E.A. Price, W.F. Schneider, J.F. Brennecke, J. Am. Chem. Soc. 132 (2010) 2116.
[54] R.K. Khanna, M.H. Moore, Spectrochim. Acta A Mol. Biomol. Spectrosc. 55A (1999) 961.
[55] E. Davarpanah, S. Hernández, G. Latini, C.F. Pirri, S. Bocchini, Advanced Sustainable Systems 4 (2020) 1900067.